

Border-collision bifurcations in a driven time-delay system

Pierce Ryan,¹ Andrew Keane,^{2,1} and Andreas Amann¹

¹*School of Mathematical Sciences, University College Cork, Cork T12 XF62, Ireland*

²*Department of Mathematics, The University of Auckland, Private Bag 92019, Auckland 1142, New Zealand*

We show that a simple piecewise-linear system with time delay and periodic forcing gives rise to a rich bifurcation structure of torus bifurcations and Arnold tongues, as well as multistability across a significant portion of the parameter space. The simplicity of our model enables us to study the dynamical features analytically. Specifically, these features are explained in terms of border-collision bifurcations of an associated Poincaré map. Given that time delay and periodic forcing are common ingredients in mathematical models, this analysis provides widely applicable insight.

Both time-delay dynamical systems, and periodically driven dynamical systems have been thoroughly studied in the literature. This can be attributed to their great relevance to real-world problems. Time-delay systems arise naturally in physical, biological or climate models due to finite propagation speed; periodic drive is ubiquitous in engineering applications and is known to generate complex resonance phenomena. However, systems that combine these two properties have received much less attention, despite being relevant in many real-world applications. In this paper, we study a simple piecewise-linear system with both time delay and periodic forcing, which exhibits interesting dynamical features as a nontrivial consequence of this combination. These features include multistabilities, Arnold tongues and torus bifurcations. Since the system is piecewise linear and contains only two parameters, many phenomena can be interpreted through an analytically derived piecewise-smooth Poincaré map and an analysis of the associated border-collision bifurcations. The analysis explains the origin of similar phenomena which has previously been observed numerically in more complicated related systems.

This article may be downloaded for personal use only. Any other use requires prior permission of the author and AIP Publishing. This article appeared in *Chaos* **30**, 023121 (2020) and may be found at <https://aip.scitation.org/doi/10.1063/1.5119982>.

I. INTRODUCTION

Periodically driven systems appear in many real-world applications. Examples include optical injection in laser systems¹, vibration-driven energy harvesting devices², injection-locked frequency dividers in electronics³, or seasonal forcing in climate systems⁴. They often give rise to interesting resonance behaviour in damped oscillators⁵ and complex synchronization patterns in self-sustained

oscillators^{6,7}.

Similarly, time-delay systems also arise in many experimental systems, for example in optics⁸, electronics⁹, neuro-science¹⁰, or climate systems¹¹, and also play an important role in chaos control, for example, through the use of time-delayed feedback control¹². From a mathematical point of view, time delay often leads to a formally infinite-dimensional phase space¹³, which considerably complicates the analysis, but allows for a rich variety of phenomena.

The combination of external forcing and time delay has been studied, for example, in the context of the Duffing oscillator¹⁴, the van der Pol oscillator¹⁵ and more recently in the context of climate systems^{16,17}. However, a general understanding of this class of dynamical systems is not yet available. The objective of the current paper is, therefore, to study the fundamental features of an elementary system with time delay and periodic forcing to obtain a broader insight into what phenomena are expected to arise as a consequence of this combination.

Let us consider a simple driven time-delay dynamical system introduced by Ghil et al.¹⁶ as a model for a climate phenomenon known as the El Niño Southern Oscillation. The system of a real variable $x \in \mathbb{R}$ is defined by

$$\dot{x}(t) = -\tanh[\kappa x(t - \tau)] + b \sin(2\pi t), \quad (1)$$

$$x(t) \in C([-\tau, 0]), \quad (2)$$

where $b \geq 0$ is the magnitude of the periodic forcing, $\tau > 0$ is the time delay of the delayed feedback, and $\kappa > 0$ is the linear slope of the delayed feedback at the origin. A solution of the system is a trajectory $x(t) \in \mathbb{R}$, $t \in \mathbb{R}$. A consequence of the reliance of the delayed feedback on a continuous function $x(t)$ over an interval $[-\tau, 0]$ is that the system has an infinite-dimensional phase-space. Another key feature of this system is that it has the symmetry $x(t) \rightarrow -x(t + \frac{1}{2})$. This model has been studied extensively by Keane et al.^{17,18}. Numerical analysis of this system demonstrated an extremely complex resonance structure¹⁷. Furthermore, the autonomous system ($b = 0$) has been studied analytically^{19,20}. In this case the trivial solution $x \equiv 0$ is only stable for $\tau < \frac{\pi}{2\kappa}$. At $\tau = \frac{\pi}{2\kappa}$, it becomes unstable, and a family of stable 4τ -periodic solutions is born.

In order to analyse the phenomena seen in this model further, let us consider a further simplification of the system by taking $\kappa \rightarrow \infty$. This has the effect of changing the delayed feedback term from $-\tanh[\kappa x(t - \tau)]$ to $-\text{sgn}[x(t - \tau)]$. We also apply the signum function to the periodic forcing to obtain the dynamical system

$$\dot{x}(t) = -\text{sgn}[x(t - \tau)] + b \text{sgn}(\sin(2\pi t)), \quad (3)$$

$$x(t) \in C([-\tau, 0]), \quad (4)$$

where $b \geq 0$ and $\tau > 0$. Critically, this simplification of the system preserves the symmetry $x(t) \rightarrow -x(t + \frac{1}{2})$. The feedback term $-\text{sgn}[x(t - \tau)]$ takes values in $\{1, 0, -1\}$. However, while the feedback can in principle be 0, this occurs only under highly specific conditions which are not considered here. The forcing term $b \text{sgn}[\sin(2\pi t)]$ takes values in $\{b, 0, -b\}$. As the forcing is 0 only at discrete times, we say that the forcing is positive for $t \bmod 1 \in [0, 0.5)$, and negative for $t \bmod 1 \in [0.5, 1)$. We now develop our method for solving the system.

II. NUMERICS

A. Iterative map

In order to solve Eqs. (3,4), we note that $\dot{x}(t)$ can only take discrete values in $\{1 + b, -1 + b, 1 - b, -1 - b\}$; therefore this continuous system can be modelled exactly as a discrete time iterative map, or Poincaré map. The state of the system at time t is a tuple of variable length

$$S(t) = (x; z_0, z_1, \dots, z_{n-1}), \quad (5)$$

where $x \in \mathbb{R}$ is the position at time t and $t - \tau < z_0 < z_1 < \dots < z_{n-1} \leq t$ are *zero elements*, which are the times at which the trajectory passed through $x = 0$ in $(t - \tau, t]$. Let n be the number of zero elements in $S(t)$. Thus, Eq. (3) may be rewritten as

$$\dot{x}(t) = -\text{sgn}[x(t)](-1)^n + b \text{sgn}[\sin(2\pi t)]. \quad (6)$$

This representation of the state of the system shows that the dimension of this system is finite, but variable. This will have a significant impact in our analysis of this system.

There are three key events that occur in a trajectory that affect $S(t)$:

1. A zero element is added. When $x(t)$ passes through $x = 0$, a zero element equal to t is appended to S , increasing n by 1; this does not immediately cause the feedback to change as the sign of $x(t)$ also changes, but it will affect \dot{x} at time $t + \tau$.
2. A zero element is removed. When $t = z_0 + \tau$, z_0 is deleted from S which decreases n by 1, resulting in a sign change of the feedback.

3. The forcing changes when $t \bmod 0.5 = 0$. While this does not affect the state directly, it changes \dot{x} , affecting the evolution of the state.

Between consecutive events, \dot{x} is constant. We construct our iterative map to move the system forward in time to the next event. The step size Δt for the iterative map is variable. One iteration of the map consists of calculating $\dot{x}(t)$, calculating the step size Δt , then calculating $S(t + \Delta t)$. This process is used to simulate the trajectory of the system from any given initial state $S(0)$ up to a maximum time T .

B. Sample solutions

We now present sample solutions which demonstrate some of the characteristic features of this system. Fig. 1 shows eight stable solutions found by simulating the system from different initial conditions and parameters (b, τ) .

There are periodic and aperiodic solutions present in the system. A periodic solution with period P is a trajectory that follows a cycle such that $S(t + P) = S(t)$. An aperiodic solution is considered to be a solution with infinite period. We label solutions by the *characteristic ratio* $P:R$, where R is the number of times the trajectory crosses from $x < 0$ to $x > 0$ in one cycle. Note that the $P:R$ notation differs from the $p:q$ notation used in some previous literature^{17,18}, where $\frac{p}{q}$ is the rotation number. We find that $P:R$ is a useful measure of a solution, for reasons that will be made clear later.

Fig. 1(a) is an example of the stable solution to the unforced system ($b = 0$). The change in the feedback occurs at a time $t + \tau$ after the trajectory passes through $x = 0$ at time t , resulting in a 4τ -periodic solution that is stable for $\tau > 0$. This is consistent with the analytic results found for the unsimplified system. We consider 4τ to be the natural period of the feedback, as the solution to the unforced system is 4τ -periodic. The characteristic ratio of this solution is $4\tau:1$.

Fig. 1(b) and Fig. 1(c) show a $4:2$ solution and a $3:1$ solution, respectively, that are stable for the same parameters. This is an example of bistability, where there are two stable solutions for the same parameters; the solution to which the system converges depends on which solution's basin of attraction the initial conditions are in. A second example of bistability is seen in Fig. 1(d) and Fig. 1(e), which show a $1:1$ solution and a $5:1$ solution, respectively, that are stable for the same parameters.

The solution in Fig. 1(f) is assumed to be aperiodic, as the system does not converge to a periodic solution after running a simulation up to $T = 100000$. By comparing the aperiodic solution to the $1:1$ solution in Fig. 1(g), we may note that the aperiodic solution and the $1:1$ solution have the same number of $x = 0$ crossings per period of the forcing. However, the $x = 0$ crossings are evenly spaced in the $1:1$ solution, but are not in the aperiodic

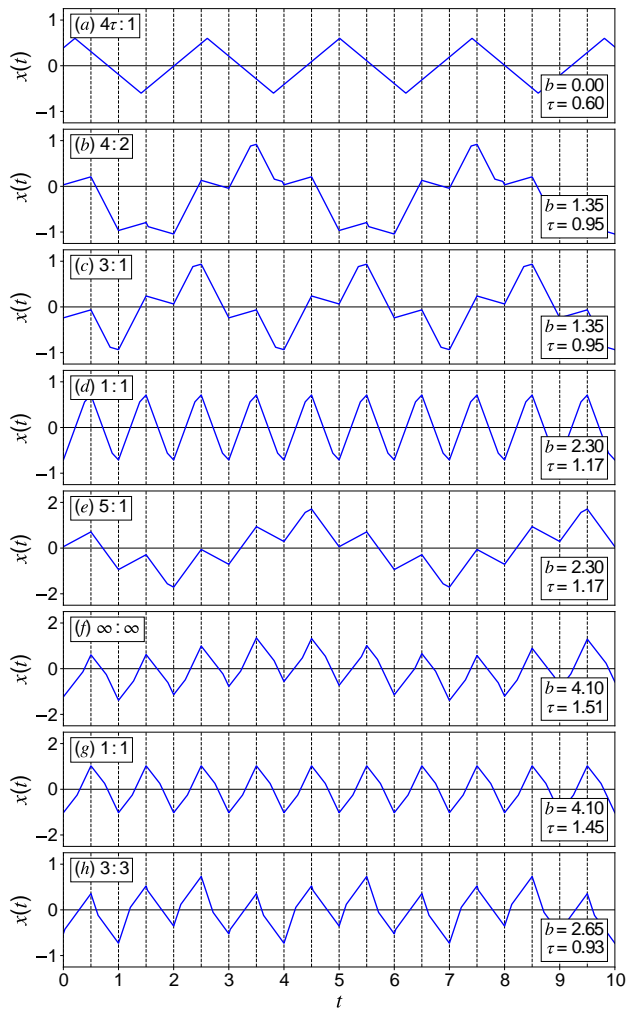


Figure 1. Sample solutions, excluding transients, obtained from simulating the system from different initial conditions and parameters (b, τ) shown in the bottom right corner of each plot. The ratio of the period of the solution to the number of crossings from $x < 0$ to $x > 0$ in one cycle is shown in the top left corner of each plot. The vertical dotted lines indicate times when the forcing changes.

solution. This may be an indicator that the aperiodic solution is related to the $1:1$ solution in Fig. 1(g). A similar observation can be made for the $3:3$ solution in Fig. 1(h) and the $1:1$ solution in Fig. 1(d). In later sections of this paper, we will investigate these relationships in detail.

C. Structure in the (b, τ) plane

Having seen some interesting features of the system, we move on to understanding the overall dynamics in the (b, τ) plane. Due to the bistability present in the system, simulating the system from arbitrary initial con-

ditions across a (b, τ) mesh would produce an inconsistent picture, as we have no prior knowledge of the basins of attraction of bistable solutions. In order to circumvent this issue, for fixed τ , the solution is swept across a range of b by iteratively simulating the system, incrementing b slightly, then simulating again using the final state of the previous simulation as the initial state of the next one. This allows a stable solution to be followed until it loses stability or ceases to exist, at which point the system converges to a nearby stable solution. By taking multiple sweeps in b for a range of fixed τ values, we obtain the $P:R$ charts shown in Fig. 2. Fig. 2(a) shows the $P:R$ chart under an upward sweep in b , from left to right. Fig. 2(b) shows the $P:R$ chart under a downward sweep in b , from right to left. This figure demonstrates many striking features of the system which will be explored in more detail.

First, let us focus our attention on the upward b sweep in Fig. 2(a). We observe that there are regions in the (b, τ) plane in which particular $P:R$ solutions exist, such as the labelled $3:1$, $5:1$, $7:1$ and $9:1$ regions on the left side of the chart. These regions are sections of Arnold tongues. An Arnold tongue is a region of the (b, τ) plane, rooted on $b = 0$, within which the feedback and the forcing synchronise to produce a solution with period equal to a rational ratio of the forcing. In piecewise-linear systems, an Arnold tongue can have shrinking points, at which the Arnold tongue has zero width. This phenomenon was first observed in the circle map²¹, and analysed in detail in the context of piecewise-linear continuous maps with single switching mechanisms^{22–24}. This produces Arnold tongues that have been compared to strings of sausages²¹. We will refer to an individual “sausage” as a *tongue*, and refer to a full “string” as an *Arnold tongue*. A notable feature of these Arnold tongues is that the characteristic ratio is different in each tongue in the string. For example, the $P = 7$ Arnold tongue is rooted on $b = 0$ at $\tau = 1.75$, and consists of the $7:1$ tongue, the $7:3$ tongue, the $7:5$ tongue, and the unlabelled $7:7$ tongue. In each Arnold tongue, the leftmost tongue is a $P:R$ tongue that is rooted on $b = 0$ at $\tau = \frac{P}{4R}$. P is the same in every tongue in the chain, but R increases the further right the tongue is in the string.

Tongues with similar characteristic ratios tend to have similar shape, with some variation. For example, the $6:2$ and $8:2$ tongues have identical shape; the $4:2$ tongue is different. The large $P:1$ tongues noted earlier have identical shape for $P > 1$. The $1:1$ Arnold tongue is unlike any other Arnold tongue in shape. For large b , the forcing dominates the feedback, which results in the system converging to the $1:1$ solution exclusively. We refer to the region in which b is large enough as the locked region, where the system is locked to the period of the forcing. The boundary of the locked region is unusual, being made up of straight lines which meet at right angles. Branching off from the horizontal lines of the boundary, there are vertical stripes in which $P:P$ solutions exist. We

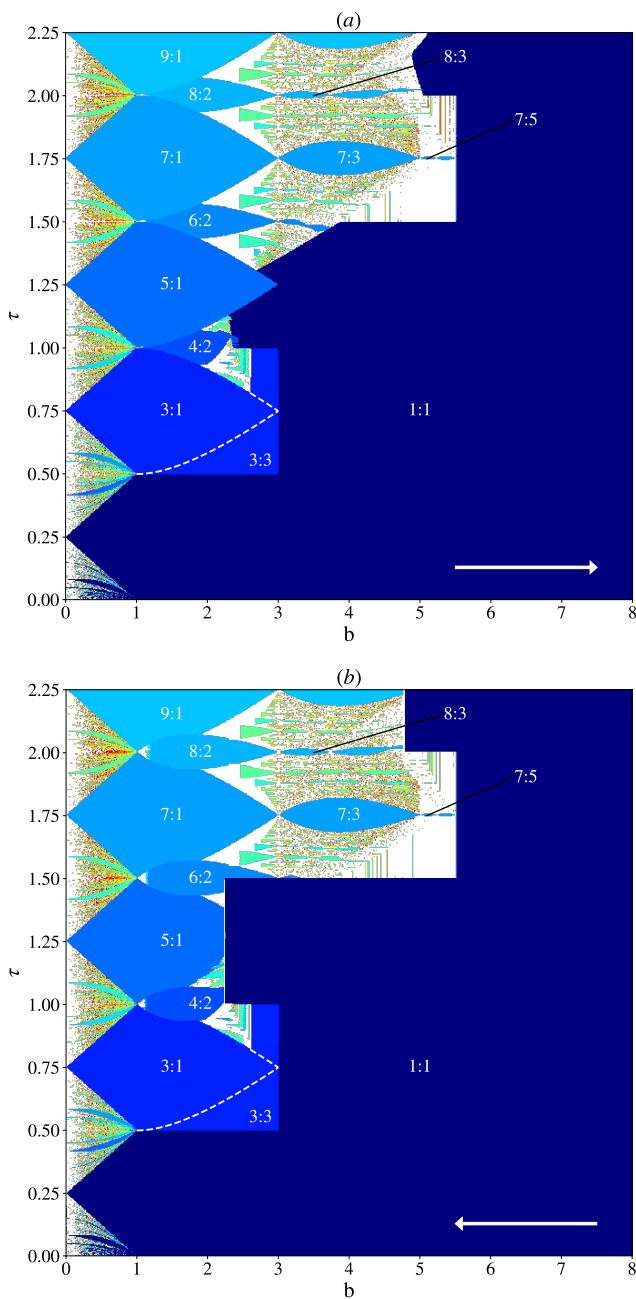


Figure 2. Colour maps showing the period of simulated solutions obtained by making 1124 sweeps of 1125 simulations of duration $T = 10000$ in $[0, 8] \times [0, 2.5]$. The white arrows indicate the direction of the sweep. Dark blue indicates $P = 1$ solutions, shading to dark red for $P = 999$ solutions. White space indicates where the solution was aperiodic, or had $P > 999$. The white text indicates the characteristic ratio of stable solutions found within the tongues. The dashed white line shows the border between the regions where the $3:1$ and $3:3$ solutions occur.

will devote considerable attention to studying the $1:1$ solution later.

Now we compare the upward b sweep in Fig. 2(a) to

the downward b sweep in Fig. 2(b). The most significant difference occurs around $(b, \tau) = (2.5, 1.25)$. In the upward sweep, the system follows the $5:1$ solution to the edge of the $5:1$ tongue, and there is a complicated region of smaller tongues and aperiodicity above the $5:1$ tongue. In the downward sweep, the system instead continues to follow the $1:1$ solution into the region where different features occurred in the upward sweep. This agrees with the bistability of the $1:1$ and $5:1$ solutions seen in Fig. 1(d,e). A less obvious difference is the bistability to the right of $b = 1$; note the apparent difference in shape of the $P:2$ and $P:1$ tongues near this line. This occurs because the $P:1$ solutions overlap with the $P:2$ solutions, in agreement with the bistability of the $4:2$ and $3:1$ solutions seen in Fig. 1(b,c). The absence of $P:1$ tongues for even P is notable. We numerically observe such solutions in simulations, but only for small $b \lesssim 0.5$ and exactly $\tau = \frac{P}{4}$.

III. DYNAMICS

Fig. 3 shows maximum charts in the (b, τ) plane overlaid with bifurcation curves. The maximum is taken as the maximum value of a solution over an interval of length 1000 after a transient of length 9000 from the same simulations that were used to generate Fig. 2. Some of the larger tongues seen in Fig. 2 can be seen without difficulty in Fig. 3 due to a large jump in maxima at the boundaries of the tongues. We note that the even $P:R$ tongues are striped horizontally; this is most evident in the $4:2$ and $8:2$ tongues. It appears that solutions with even P or R are not invariant under the symmetry $x(t) \rightarrow -x(t + \frac{1}{2})$; rather there exists a pair of symmetry-related counterpart solutions, each with a different maximum value. The system converges to one of these solutions depending on initial conditions, and remains at that solution until swept out of the tongue, resulting in stripes parallel to the direction of the sweep. This feature was also observed in the smooth system (1,2) by Keane, Krauskopf, and Postlethwaite¹⁷.

We will devote the rest of this section to deriving and characterising the bifurcation curves plotted in Fig. 3. In order to do so, we first need to establish a systematic method of analysing solutions. We apply this method to develop Poincaré maps and border collision maps through which we study the bifurcations present in this system.

A. Symbolic representation

We require a robust framework under which we can analyse the dynamics of this system. We note that the characteristic ratio does not distinguish between the two different forms of the $1:1$ solution shown in Fig. 1(d,g). Observing the order in which the feedback and forcing change after the trajectory passes through $x = 0$, we note that the feedback changes before the forcing in Fig. 1(d),

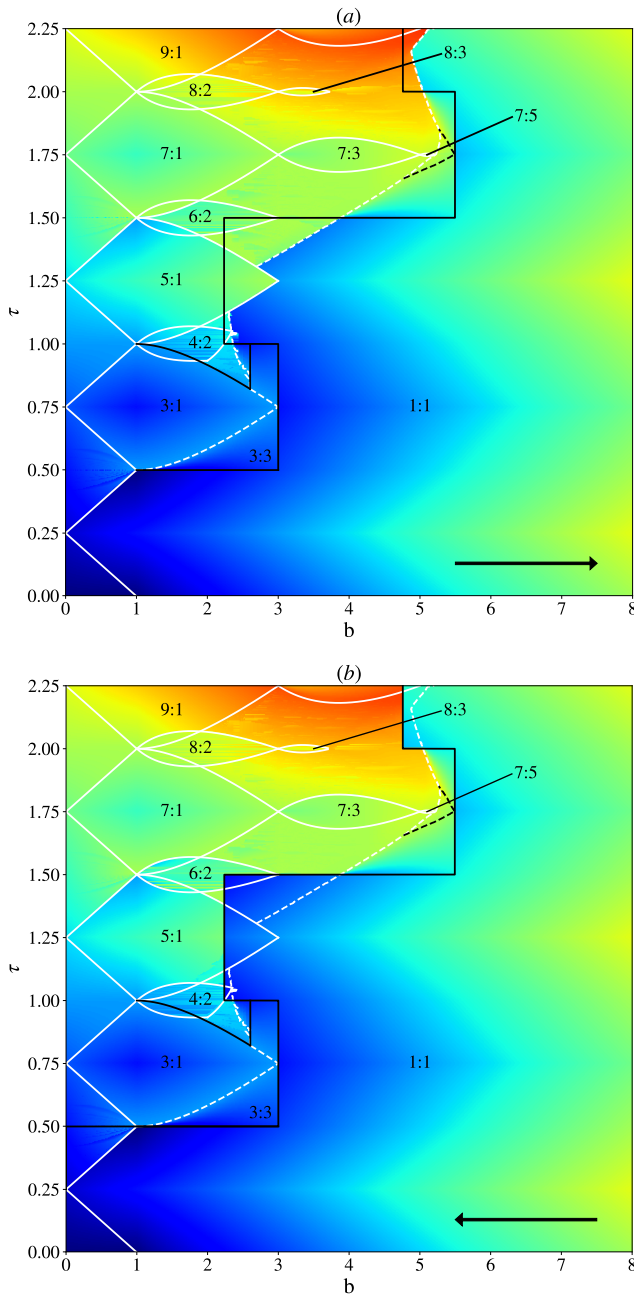


Figure 3. Maximum charts in the (b, τ) plane overlaid with bifurcation curves. Blue indicates a low maximum, red indicates a high maximum. The black arrows indicate the direction in which solutions were swept. The black text indicates the ratio of the period of the solution to the number of Z symbols in the sequence for the stable solution within the associated tongue. BCSN bifurcations are shown in solid white, and T bifurcations are shown in solid black. The DD curve is shown in dashed white.

and after the forcing in Fig. 1(g). In order to precisely capture these differences, a more explicit labelling system is required. We therefore adopt a symbolic representation of solutions. Symbolic representations have previ-

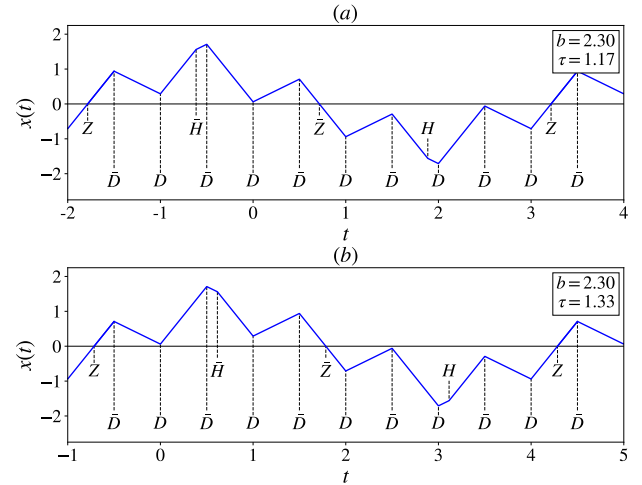


Figure 4. Derivation of the symbolic representations of the 5 : 1 solution.

ously been used to great effect in the study of iterative maps^{23,25}.

Let a solution be represented by a sequence of events $\dots X_1 X_2 \dots X_n \dots$ where $X_i \in \{D, \bar{D}, Z, \bar{Z}, H, \bar{H}\}$. D denotes a transition of the forcing from $-b$ to b , Z denotes a transition from $x < 0$ to $x > 0$, and H denotes a transition of the feedback from -1 to 1 . A bar over a symbol causes it to denote the opposite transition; a symbol with two bars over it is the same as the symbol unbarred. Fig. 4(a) shows the 5 : 1 solution seen Fig. 1(e), labelled with the events that occur in the trajectory. As this solution is periodic, the sequence repeats, so we abbreviate the sequence of events representing the solution to a minimal repeating sequence $[Z, \bar{D}, D, \bar{H}, \bar{D}, D, \bar{D}, \bar{Z}, D, \bar{D}, H, D, \bar{D}, D]$. In general, a $P : R$ solution is represented by a minimal repeating sequence of events $[X_1, X_2, \dots, X_n]$ containing:

- P D events and P \bar{D} events,
- R Z events and R \bar{H} events,
- R \bar{Z} events and R H events.

Every cyclic permutation of a sequence represents the same solution. For the sake of consistency, all sequences begins with a Z . We observe that the 5 : 1 solution shown in Fig. 4(a) is invariant under the symmetry $x(t) \rightarrow -x(t + \frac{1}{2})$; this causes the second half of the sequence $[Z, \bar{D}, D, \bar{H}, \bar{D}, D, \bar{D}, \bar{Z}, D, \bar{D}, H, D, \bar{D}, D]$ to be the same as the first half with all symbols barred. We abbreviate $[Z, \bar{D}, D, \bar{H}, \bar{D}, D, \bar{D}, \bar{Z}, D, \bar{D}, H, D, \bar{D}, D]$ as $[Z, \bar{D}, D, \bar{H}, \bar{D}, D, \bar{D}]^-$ for convenience. In general, a $P : R$ solution of the form $[X_1, X_2, \dots, X_n, \bar{X}_1, \bar{X}_2, \dots, \bar{X}_n]$ can also be represented by a half-sequence $[X_1, X_2, \dots, X_n]^-$.

A sequence is considered *legal* within a subset of the (b, τ) plane if it represents a solution that exists within

that subset. Each $P : R$ solution is represented by a set of legal sequences, each one existing in a unique subset of the (b, τ) plane. The union of these subsets is the region in which the solution exists. The 5 : 1 solution exists within the 5 : 1 tongue shown in Fig. 2(a). It is represented by the half-sequences $[Z, \bar{D}, D, \bar{H}, \bar{D}, D, \bar{D}]^-$ for $\tau \leq 1.25$ and $[Z, \bar{D}, D, \bar{D}, \bar{H}, D, \bar{D}]^-$ for $\tau \geq 1.25$, as shown in Fig. 4. At $\tau = 1.25$, the increasing time delay between Z and \bar{H} causes \bar{H} to swap with \bar{D} , changing the sequence. Determining whether a given sequence is legal within a subset of the (b, τ) plane is a nontrivial problem. Appendix A presents a general method to determine whether a sequence is legal for a given (b, τ) , which can also be used to calculate a solution analytically from a sequence for a given (b, τ) . This method was used to plot the solutions in Figs. 4,5 and the bifurcation curves in Fig. 3.

B. Torus bifurcation of the 1 : 1 solution

We now apply our sequence representation in analysing the 1 : 1 solution; specifically, we determine what happens at the vertical black lines along the boundary of the locked region in Fig. 3. Consider the set of half-sequences that represent the 1 : 1 solution. Each half-sequence contains one Z or \bar{Z} , one H or \bar{H} , and one D or \bar{D} . We need only consider half-sequences starting with Z , as $[X_1, X_2, X_3]^- = [X_3, X_1, X_2]^- = [X_2, X_3, X_1]^-$. There are only eight possibilities: $[Z, H, D]^-$, $[Z, D, H]^-$, $[Z, \bar{H}, D]^-$, $[Z, D, \bar{H}]^-$, $[Z, H, \bar{D}]^-$, $[Z, \bar{D}, H]^-$, $[Z, \bar{H}, \bar{D}]^-$, $[Z, \bar{D}, \bar{H}]^-$. $[Z, H, D]^-$ and $[Z, D, H]^-$ are not legal, as they require Z to occur when $\dot{x} < 0$, which is impossible. Similarly, $[Z, \bar{H}, D]^-$ and $[Z, D, \bar{H}]^-$ are legal only for $b < 1$, and $[Z, \bar{D}, H]^-$ and $[Z, H, \bar{D}]^-$ are legal only for $b > 1$. The 1 : 1 solutions shown in Fig. 1 are $[Z, \bar{H}, \bar{D}]^-$ in Fig. 1(d) and $[Z, \bar{D}, \bar{H}]^-$ in Fig. 1(g). In the case $b > 1$, the sequence representing the 1 : 1 solution is restricted by τ in the following way:

$$\begin{aligned} & [Z, \bar{H}, \bar{D}, \bar{Z}, H, D] \text{ for } \tau \bmod 1 \in [0, 0.25), \\ & [Z, \bar{D}, \bar{H}, \bar{Z}, D, H] \text{ for } \tau \bmod 1 \in [0.25, 0.5), \\ & [Z, H, \bar{D}, \bar{Z}, \bar{H}, D] \text{ for } \tau \bmod 1 \in [0.5, 0.75), \\ & [Z, \bar{D}, H, \bar{Z}, D, \bar{H}] \text{ for } \tau \bmod 1 \in [0.75, 1). \end{aligned} \quad (7)$$

This can be explained by observing that for small τ , \bar{H} must follow the Z that created it almost immediately. As τ increases, \bar{H} drifts further away from Z in the sequence, drifting past \bar{D} at $\tau = 0.25$. At $\tau = 0.5$, \bar{H} drifts past the subsequent \bar{Z} . At $\tau = 0.75$, \bar{H} drifts past the subsequent D . At $\tau = 1$, the \bar{H} created at Z drifts past the subsequent Z , and the pattern repeats. At the same time, the same drift pattern occurs between \bar{Z} and H . We now apply this information to analyse the 1 : 1 solution.

We construct a Poincaré map on the 1 : 1 solution. Let t_z be a time on the 1 : 1 solution at which $x = 0$; then the state of the system at time t_z is

$$S(t_z) = (0; z_0, z_1, \dots, z_{n-2}, t_z)^T. \quad (8)$$

As $x = 0$ at $t = t_z$, we drop x and rewrite the state as

$$S_z = (z_0, z_1, \dots, z_{n-2}, t_z)^T. \quad (9)$$

Let t_z^* be the time on the 1 : 1 solution at which $x = 0$ immediately after t_z . Then the state of the system at time t_z^* is

$$S_z^* = (z_1, z_2, \dots, t_z, t_z^*)^T. \quad (10)$$

As the 1 : 1 solution is invariant under the symmetry $x(t) \rightarrow -x(t + \frac{1}{2})$, it has the property

$$S_z = \begin{pmatrix} z_0 \\ z_1 \\ \dots \\ z_{n-2} \\ t_z \end{pmatrix} = \begin{pmatrix} z_1 - \frac{1}{2} \\ z_2 - \frac{1}{2} \\ \dots \\ t_z - \frac{1}{2} \\ t_z^* - \frac{1}{2} \end{pmatrix} = S_z^* - \frac{1}{2}. \quad (11)$$

We define a Poincaré map $\mathbb{P} : S_z \rightarrow S_z^* - \frac{1}{2}$ so that the 1 : 1 solution is a fixed point of \mathbb{P} . Therefore, \mathbb{P} is defined by

$$\mathbb{P} \begin{pmatrix} z_0 \\ z_1 \\ \dots \\ z_{n-2} \\ t_z \end{pmatrix} = \begin{pmatrix} z_1 - \frac{1}{2} \\ z_2 - \frac{1}{2} \\ \dots \\ t_z - \frac{1}{2} \\ t_z^* - \frac{1}{2} \end{pmatrix}. \quad (12)$$

For the purpose of deriving \mathbb{P} , we will assume w.l.o.g. that the trajectory is transitioning from $x < 0$ to $x > 0$ at $t_z \in [0, 0.5)$. Let $t_h \in [t_z, t_z^*)$ be the time at which the feedback changes. First, we consider the case where $\tau < 0.5$; then the zero element generated at t_z is consumed at $t_h = t_z + \tau$. Then \mathbb{P} is one-dimensional as S_z has only one variable, t_z . We write the one-dimensional map as

$$\mathbb{P}(t_z) = t_z^* - \frac{1}{2}. \quad (13)$$

If $\tau < 0.5$, then the solution is represented by the sequence $[Z, \bar{H}, \bar{D}]^-$; therefore, the feedback is positive for $t \in [t_z, t_h)$. We write an equation for the displacement of the trajectory between t_z and t_z^* as

$$b \left(\frac{1}{2} - t_z \right) - b \left(t_z^* - \frac{1}{2} \right) + (t_h - t_z) - (t_z^* - t_h) = 0. \quad (14)$$

We substitute $t_h = t_z + \tau$ and solve for $t_z^* - \frac{1}{2}$ to obtain

$$\mathbb{P}(t_z) = - \left(\frac{b-1}{b+1} \right) t_z + \frac{b+2\tau}{b+1} - \frac{1}{2}. \quad (15)$$

As $\left| \frac{b-1}{b+1} \right| < 1$ for $b \geq 0$, \mathbb{P} is stable for $\tau < \frac{1}{2}$.

If $\tau \in [0.5, 1)$, then t_h was generated, not at t_z , but at the previous $x = 0$ crossing z_0 . Then \mathbb{P} is two-dimensional as S_z has two variables, and the feedback is negative for $t \in [t_z, t_h)$, where $t_h = z_0 + \tau$. These conditions can be generalised for larger τ . The dimension of the system is $n = \lceil 2\tau \rceil$, where $\lceil 2\tau \rceil$ is the smallest integer greater than 2τ ; then the feedback for $t \in [t_z, t_h)$ is $(-1)^{n-1}$. We can then generalise Eq. (14) for arbitrary n and solve for $t_z^* - \frac{1}{2}$ to obtain

$$t_z^* - \frac{1}{2} = -t_z + \frac{b + 2t_h(-1)^{n-1}}{b + (-1)^{n-1}} - \frac{1}{2}. \quad (16)$$

For $\tau > \frac{1}{2}$, \mathbb{P} can be written as

$$\mathbb{P}(S_z) = AS_z + B, \quad (17)$$

where A is an $n \times n$ matrix

$$A = \begin{pmatrix} 0 & 1 & 0 & \cdots & 0 \\ \vdots & 0 & \ddots & \ddots & \vdots \\ \vdots & \vdots & \ddots & \ddots & 0 \\ 0 & 0 & \cdots & 0 & 1 \\ \frac{2(-1)^{n-1}}{b+(-1)^{n-1}} & 0 & \cdots & \cdots & -1 \end{pmatrix}, \quad (18)$$

B is given in Appendix B. Note that A only depends on the parameter b and not on τ . This means that for fixed n , the value of b at which the fixed point of \mathbb{P} is bifurcating, b_{bif} , is constant. By solving the characteristic equation, we calculate

$$b_{\text{bif}}(n) = \frac{1}{\cos\left(\frac{\pi(n-1)}{2n-1}\right)} - (-1)^{n-1}, \quad (19)$$

where $n = \lceil 2\tau \rceil$. Full calculations may be found in Appendix B. The curve $(b_{\text{bif}}(\lceil 2\tau \rceil), \tau)$ can be seen plotted as black vertical lines against maximum charts in Fig. 3. If we examine the maximum chart where b is swept from right to left, we see that the system ceases to converge to the 1:1 solution along this curve. We now know that this is because the fixed point of \mathbb{P} , and hence the 1:1 solution, loses stability at $b = b_{\text{bif}}$. By calculating the eigenvalues of \mathbb{P} explicitly for $n = 2$ and $n = 3$, we find that the loss of stability occurs because a pair of complex conjugate eigenvalues $\lambda_{1,2}$ cross $|\lambda| = 1$. Therefore the fixed point of \mathbb{P} loses stability due to a Neimark-Sacker (NS) bifurcation²⁶. As \mathbb{P} is a Poincaré map on a periodic orbit, a NS bifurcation of the fixed point of \mathbb{P} corresponds to a torus (T) bifurcation of the 1:1 solution. However, \mathbb{P} only shows the existence of the T bifurcation along the vertical sections of the boundary of the locked region, where n is constant and \mathbb{P} is smooth. To fully understand the horizontal sections of the boundary, we must look to non-smooth bifurcation theory.

IV. BORDER-COLLISION BIFURCATIONS

The Arnold tongues seen in Fig. 2 have sharply defined boundaries, made up of curves and straight lines.

We seek to determine what happens to solutions at these boundaries and derive analytic expressions for the boundaries using Poincaré maps.

By simulating solutions near the boundaries of the Arnold tongues, we observe that moving closer to the boundaries causes a D or \bar{D} to move closer to $x = 0$. An example of this is Fig. 4(a), where the D at $t = 0$ in the 5:1 solution occurs for $x > 0$ near $x = 0$. If this D crossed $x = 0$ and occurred at $x < 0$, this would significantly impact the feedback. There would be two additional $x = 0$ crossings in the trajectory, changing the D to $\bar{Z}DZ$ and adding a H and a \bar{H} elsewhere in the sequence. Therefore, when we construct a Poincaré map to describe the dynamics of the system close to the boundary of such a tongue, the map must have a border at $x = 0$, such that the map is continuous across the border but not differentiable at the border. Such maps, and the associated border-collision bifurcations, have recently received systematic analysis in the literature²⁷⁻³⁵.

A. Border-collision saddle-node bifurcation of the 5:1 and 5:3 solutions

We construct a Poincaré map \mathbb{B} on the 5:1 and 5:3 solutions represented by $[Z, \bar{D}, D, \bar{H}, \bar{D}, D, \bar{D}]^-$ and $[Z, \bar{D}, \bar{H}, H, D, \bar{H}, \bar{D}, \bar{Z}, D, Z, \bar{D}]^-$ respectively, which can be seen in Fig. 5(a), such that our fixed point is the state of the system at time $t = 0$, at the position x_D at which the D that will cross $x = 0$ occurs. As the \bar{H} created at Z occurs before this D , \mathbb{B} is one-dimensional. We divide \mathbb{B} into \mathbb{B}^+ and \mathbb{B}^- for $x \geq 0$ and $x < 0$ respectively. The 5:1 and 5:3 solutions are invariant under the symmetry $x(t) = -x(t + \frac{1}{2})$; therefore we construct our map $\mathbb{B} : x_D(0) \rightarrow -x_D(\frac{5}{2})$. \mathbb{B}^+ is a map on the solution represented by $[Z, \bar{D}, D, \bar{H}, \bar{D}, D, \bar{D}]^-$. Following the blue curve in Fig. 5(b), we can derive

$$\mathbb{B}^+(x_D) = -\left(\frac{b-1}{b+1}\right)x_D + \frac{2b}{b+1} - \frac{b+5}{2} + 2\tau. \quad (20)$$

\mathbb{B}^- is a map on the 5:3 solution represented by $[Z, \bar{D}, \bar{H}, H, D, \bar{H}, \bar{D}, \bar{Z}, D, Z, \bar{D}]^-$, which is shown in Fig. 5(b) in red. The feedback change due to the trajectory dipping below $x = 0$ occurs at some $t \in (1, 1.5)$ has duration $\frac{-2bx}{b^2-1}$; \mathbb{B}^- is otherwise identical to \mathbb{B}^+ . Thus we derive \mathbb{B} as

$$\mathbb{B}(x_D) = \begin{cases} -\left(\frac{b-1}{b+1}\right)x_D + \frac{2b}{b+1} - \frac{b+5}{2} + 2\tau & x_D \geq 0 \\ \left(\frac{4b}{b^2-1} - \frac{b-1}{b+1}\right)x_D + \frac{2b}{b+1} - \frac{b+5}{2} + 2\tau & x_D < 0 \end{cases} \quad (21)$$

By setting $x_D = 0$ and solving \mathbb{B} for τ , we obtain the curve $\tau = \frac{b^2+2b+5}{4(b+1)}$. This matches the lower right boundary of the 5:1 tongue spanning from (1, 1) to (3, 1.25). For $b \in [1, 3]$ and $\tau \in \left[\frac{b^2+2b+5}{4(b+1)}, 1.25\right]$, \mathbb{B} has two fixed points; a stable fixed point that exists for $x_D \geq 0$ and

an unstable fixed point that exists for $x_D \leq 0$. These two fixed points collide and vanish at the border $x_D = 0$ at $\tau = \frac{b^2+2b+5}{4(b+1)}$ in a border-collision saddle-node (BCSN) bifurcation²⁸. Hence the 5 : 1 tongue is bounded by a BCSN bifurcation. Fig. 5(b,e,f) shows the BCSN bifurcation of the 5 : 1 and 5 : 3 solutions.

We generalise \mathbb{B} for every $P : 1$ tongue for odd $P \geq 5$ as

$$\mathbb{B}_P(x_D) = \begin{cases} -\left(\frac{b-1}{b+1}\right)x_D + \frac{2b}{b+1} - \frac{b+|P-4\tau|}{2} & x_D \geq 0 \\ \left(\frac{4b}{b^2-1} - \frac{b-1}{b+1}\right)x_D + \frac{2b}{b+1} - \frac{b+|P-4\tau|}{2} & x_D < 0 \end{cases} \quad (22)$$

where $|P - 4\tau|$ is the term that causes the $P : 1$ tongues to be symmetric across $\tau = \frac{P}{4}$. By setting $x_D = 0$, we calculate the boundaries of all $P : 1$ tongue for odd $P \geq 5$ and $b \in [1, 3]$ as

$$\tau_P(b) = \frac{P}{4} \pm \frac{3b - b^2}{4(b+1)}. \quad (23)$$

We find that this phenomenon persists throughout the system. The vast majority of tongues investigated are bounded by BCSN bifurcations occurring when a D crosses $x = 0$. For $b > 1$, a stable $P : R$ solution and an unstable $P : R + 2$ solution undergo a SN bifurcation when a D crosses $x = 0$ if the solution has the symmetry $x(t) = -x(t + \frac{P}{2})$. Otherwise, the stable $P : R$ solution undergoes a SN bifurcation with an unstable $P : R + 1$ solution when a D crosses $x = 0$.

For $b < 1$, the mechanism by which BCSN bifurcations occur is slightly different. Instead of a D crossing $x = 0$ and adding new symbols to the sequence, D instead crosses $x = 0$ by swapping order with an existing Z . The stable 5 : 1 solution $[Z, \bar{D}, D, \bar{H}, \bar{D}, D, \bar{D}]^-$ undergoes a BCSN bifurcation with the unstable 5 : 1 $[Z, D, \bar{D}, D, \bar{H}, \bar{D}, D]^-$ at $(b, \frac{5-b}{4})$, $b < 1$, as shown in Fig. 5(a,c,d). While the unstable 5 : 1 and 5 : 3 solutions shown in Fig. 5 are two different solutions under our sequence representation, they are identical at $b = 1$, where a D passes through $x = 0$ without a bifurcation. A noteworthy feature of the BCSN bifurcations at the boundary of the 5 : 1 tongue is that the pair of D events which collide at $x = 0$ is different for $b < 1$ and $b > 1$, as seen in Figure Fig. 5(a,b,c,e). Generally, for $b < 1$, a stable $P : 1$ solution undergoes a BCSN bifurcation with an unstable $P : 1$ solution. Again, we produce a general form for the curves where a $P : 1$ solution undergoes a BCSN bifurcation for odd $P \geq 1$ and $b \in [0, 1]$ as

$$\tau_P(b) = \frac{P \pm b}{4}. \quad (24)$$

The 1 : 1 solution is a special case. The stable $[Z, \bar{H}, \bar{D}]^-$ solution and the unstable $[Z, D, \bar{H}]^-$ undergo a BCSN bifurcation along $(b, \frac{n}{2} + \frac{1-b}{4})$, $b < 1$, $n \in \mathbb{Z}^+$. The stable $[Z, \bar{D}, \bar{H}]^-$ solution and the unstable $[Z, \bar{H}, D]^-$

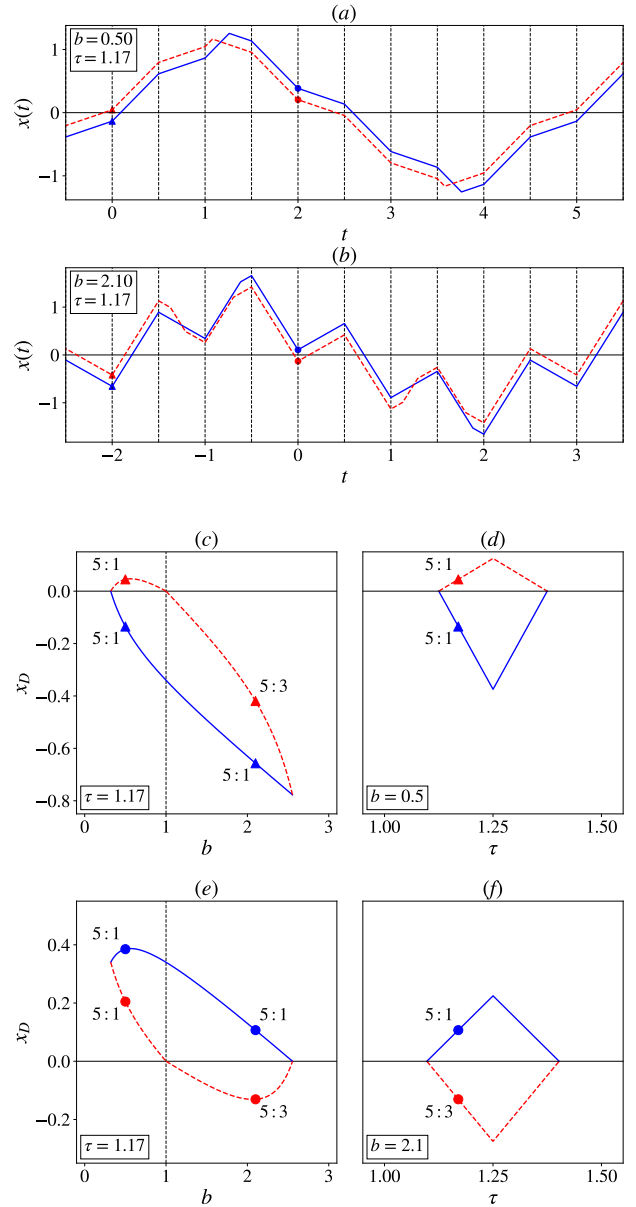


Figure 5. BCSN bifurcations at the boundary of the 5 : 1 tongue. The stable solution is plotted in solid blue, while the unstable solution is plotted in dashed red. In (a), the stable 5 : 1 solution $[Z, \bar{D}, D, \bar{H}, \bar{D}, D, \bar{D}]^-$ and the unstable 5 : 1 solution $[Z, D, \bar{D}, D, \bar{H}, \bar{D}, D]^-$ are plotted close to $(b, \frac{5-b}{4})$. In (b), the stable 5 : 1 solution $[Z, \bar{D}, D, \bar{H}, \bar{D}, D, \bar{D}]^-$ and the unstable 5 : 3 solution $[Z, \bar{D}, \bar{H}, H, D, \bar{H}, \bar{D}, \bar{Z}, D, Z, \bar{D}]^-$ are plotted close to $(b, \frac{b^2+2b+5}{4(b+1)})$. The D events associated with the BCSN bifurcation for $b < 1$ are plotted as triangles, while those associated with the BCSN bifurcation for $b > 1$ are plotted as circles; (c), (d), (e) and (f) show their evolution as b and τ vary.

undergo a BCSN bifurcation along $(b, \frac{n}{2} + \frac{1+b}{4})$, $b < 1$, $n \in \mathbb{Z}^+$.

A selection of these curves can be seen plotted in solid white in Fig. 3. There is a conspicuous outlier to this pattern. The 3 : 1 solution does not undergo a BCSN bifurcation at the right boundary of the 3 : 1 tongue for $b > 1$. We will now investigate why this is the case.

B. Border-collision torus bifurcation of the 3 : 1 solution

Fig. 2 shows that the 3 : 1 tongue has the same shape as the other $P : 1$ tongues, rooted at $\tau = 0.75$. Along some of the boundary, the 3 : 1 solution changes to the 3 : 3 solution without bifurcation. We test the observed sequences which represent the 3 : 3 solution and find that the 3 : 3 solution exists in the region $[1, 3] \times [0.5, 1]$ outside of the 3 : 1 tongue. However, the 3 : 3 solution is not always stable; this can be seen in the top half of the 3 : 3 region in Fig. 2. In order to investigate this phenomenon, we construct a Poincaré map \mathbb{T} by a similar method as for the BCSN bifurcation. For $\tau > 0.75$, the 3 : 1 solution is represented by $[Z, \bar{D}, D, \bar{H}, \bar{D}]^-$ from which we derive \mathbb{T}^+ for $x_D \geq 0$. For $x_D < 0$, the sequence changes to $[Z, \bar{H}, H, \bar{D}, \bar{Z}, D, Z, \bar{H}, \bar{D}]^-$, from which we derive \mathbb{T}^- . There is a significant difference however; the 3 : 1 solution is one-dimensional, but for $\tau > 0.75$, the 3 : 3 solution is two-dimensional. This occurs because the additional \bar{H} and H events occur between the D that crosses $x = 0$ and the Z present in both sequences. Therefore, we also need to know the time $t_{\bar{H}}$ at which the \bar{H} present in both sequences occurs. We derive $\mathbb{T} : (x_D, t_{\bar{H}})^T \rightarrow (x_D^*, t_{\bar{H}}^* - \frac{3}{2})^T$ as

$$\mathbb{T} \begin{pmatrix} x_D \\ t_{\bar{H}} \end{pmatrix} = \begin{cases} \begin{pmatrix} -1 & -2 \\ \frac{1}{b+1} & \frac{2}{b+1} \end{pmatrix} \begin{pmatrix} x_D \\ t_{\bar{H}} \end{pmatrix} + C & x_D \geq 0 \\ \begin{pmatrix} \frac{4b}{b^2-1} & -1 & -2 \\ \frac{1}{b+1} & \frac{2}{b+1} \end{pmatrix} \begin{pmatrix} x_D \\ t_{\bar{H}} \end{pmatrix} + C & x_D < 0 \end{cases} \quad (25)$$

where $C = \begin{pmatrix} \frac{3-b}{b+1} \\ \frac{2}{b+1} + \tau - \frac{3}{2} \end{pmatrix}$. Note that \mathbb{T}^+ has two rows which are multiples of each other; this is due to the 3 : 1 solution being one-dimensional, and results in a 0 eigenvalue. By setting $x_D = 0$ and solving \mathbb{T} for τ , we obtain the curve $\tau = \frac{3}{4} + \frac{3b-b^2}{4(b+1)}$, which matches the upper right boundary of the 3 : 1 tongue spanning from $(1, 1)$ to $(3, 0.75)$. \mathbb{T} has a single fixed point which crosses $x_D = 0$ at the boundary of the 3 : 1 tongue. For $x_D > 0$ the fixed point is always stable. For $x_D < 0$ the fixed point is stable for $b > 2.6038$, and loses stability when a pair of complex conjugate eigenvalues pass through $|\lambda| = 1$, resulting in a NS bifurcation at $b = 2.6038$. $|\lambda_{\pm}| < 1$ for $b > 2.6038$. Therefore, for $\tau > 0.75$ the 3 : 3 solution is stable for $b > 2.6038$. This agrees with the shape of the region in which the 3 : 3 solution is observed in Fig. 2.

For $b < 2.6038$, we observe an interesting interaction between \mathbb{T}^+ and \mathbb{T}^- . As \mathbb{T}^+ has a 0 eigenvalue, any point $(x_D, t_{\bar{H}})$ for $x_D > 0$ is mapped directly to a nullcline on

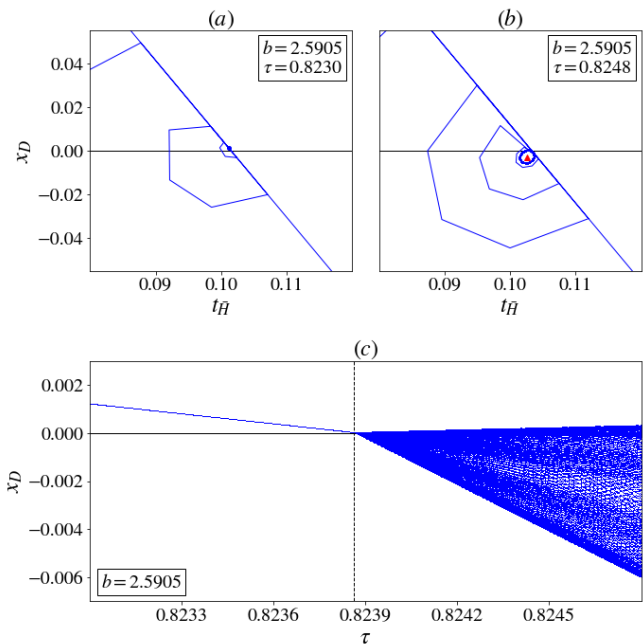


Figure 6. Border-collision Neimark-Sacker (BCNS) bifurcation of the fixed point of the 3 : 1 solution. The upper two plots show the BCNS bifurcation of the half-period map \mathbb{T} . The lower plot is based on simulation using our iterative map, and shows the stable closed invariant curve expanding from the fixed point from $x = 0$. The fixed point is plotted as a blue circle where it is stable, and as a red triangle where it is unstable.

which the fixed point sits for $x_D > 0$. The trajectory then undergoes decaying oscillations to the fixed point in the nullcline. However, if the fixed point is close to $x_D = 0$, \mathbb{T}^+ can map the point into $x_D < 0$, where the nullcline does not exist. In the absence of a stable fixed point at $x_D < 0$, the trajectory starts to spiral out to infinity. As this spiral must cross $x_D = 0$ eventually, the trajectory is caught by the nullcline again, causing an interesting half-spiral attraction. When the fixed point is at $x_D < 0$, the trajectory converges to a stable attractor that strikes the nullcline at multiple points. Fig. 6(a,b) show the interaction between \mathbb{T}^+ and \mathbb{T}^- . Fig. 6(c) shows the results of simulations in a (b, τ) sweep that crosses the boundary of the 3 : 1 Arnold tongue. The simulated results agree with those derived from \mathbb{T} , and confirm that the closed invariant curve is born from the fixed point as it crosses $x_D = 0$. We consider this to be a border-collision Neimark-Sacker (BCNS) bifurcation of \mathbb{T} , similar to that seen by Meiss³². It corresponds to a border-collision torus (BCT) bifurcation of the 3 : 1 solution in the continuous system. The BCT bifurcation is supercritical, as a stable closed invariant curve expands from the fixed point when it becomes unstable. The BCT bifurcation of the 3 : 1 solution and the \mathbb{T} bifurcation of the 3 : 3 solution are plotted in black in Fig. 3.

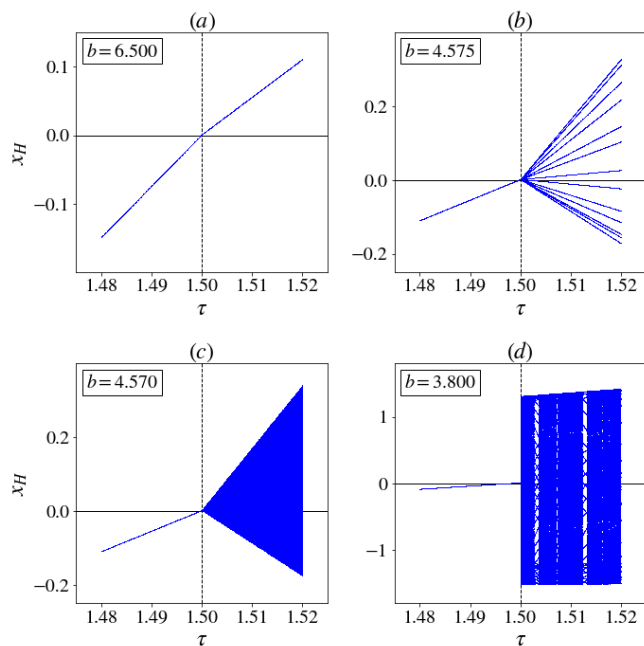


Figure 7. x -coordinates of H events from simulations. The four plots show the different cases of the $1:1$ solution at the border.

C. Border-collision torus bifurcation of the $1:1$ solution

Now that we have studied the BCT bifurcation of the $3:1$ solution, we return to the $1:1$ solution. Previously we noted that the Poincaré map \mathbb{P} only proved the existence of the torus bifurcation along the vertical boundaries of the locked region. We can now consider the horizontal boundaries in terms of border collisions. Recall that the $1:1$ solution is represented by four different sequences. At $\tau = \frac{n}{2}$, $n \in \mathbb{N}$, the sequence representing the $1:1$ solution changes when a H and a \bar{H} cross $x = 0$. This results in a change in the dimension of \mathbb{P} . Let \mathbb{P}_n denote \mathbb{P} when \mathbb{P} contains an $n \times n$ matrix. When τ increases past $\tau = \frac{n}{2}$, \mathbb{P} changes from \mathbb{P}_n to \mathbb{P}_{n+1} . Let us consider x_H , the position of the H event, as the fixed point of the map. Then $x_H = 0$ when \mathbb{P} changes from \mathbb{P}_n to \mathbb{P}_{n+1} , resulting in a border collision at $x_H = 0$. Fig. 7 shows four cases that occur in the border collision when we sweep across the border $\tau = 1.5$ for fixed b .

Fig. 7(a) shows the stable $1:1$ solution remaining stable, as both \mathbb{P}_3 and \mathbb{P}_4 are stable at $b = 6.5$. Fig. 7(b) shows the stable $1:1$ solution becoming unstable, generating a $13:13$ solution in a supercritical BCT bifurcation. This solution exists in one of the vertical stripes we noted in Fig. 2. Fig. 7(c) shows the stable $1:1$ solution becoming unstable, generating an aperiodic solution in a supercritical BCT bifurcation, showing that there are gaps between the vertical stripes. Fig. 7(d) shows the stable $1:1$ solution becoming unstable; however, the aperiodic solution that the system converges to afterwards is not generated at the border, indicating that the BCT bi-

furcation is subcritical at this point. Therefore the BCT bifurcation of the $1:1$ solution must change criticality at some point along $\tau = 1.5$. The BCT bifurcation of the $1:1$ solution produces the horizontal black lines in Fig. 3, completing the boundary of the locked region.

We examine the difference in maxima of nearby solutions on either side of $\tau = 1.5$ in Fig. 3(b). The point $(b, \tau) = (1.5, 3.86)$ stands out; the difference in maxima is sudden to the left of that point, and gradual to the right. The gradual change in maxima occurs where the BCT bifurcation is supercritical, and the abrupt change in maxima occurs where the BCT bifurcation is subcritical, as illustrated by Fig. 7(b-d). We note that $(b, \tau) = (1.5, 3.86)$ forms one corner of a roughly triangular region containing vertical $P:P$ stripes seen in Fig. 2; every $P:R$ solution in this region is $P:P$. This leads us to the dashed white curve in Fig. 3. We refer to this curve as the $D\bar{D}$ curve. To the right of the $D\bar{D}$ curve, all D events occur at $x < 0$ and all \bar{D} events occur at $x > 0$, and so a legal sequence cannot contain a D adjacent to a \bar{D} ; a $P:R$ solution in this region must, therefore, be $P:P$. To the left of the $D\bar{D}$ curve, a legal sequence representing a solution can contain a D adjacent to a \bar{D} ; we refer to such a solution as a $D\bar{D}$ solution. The point at which the BCT bifurcation changes criticality occurs where the $D\bar{D}$ curve intersects the boundary of the locked region.

As noted previously, when sweeping from right to left, the system converges to the $1:1$ solution until it becomes unstable at the T bifurcation. Now, we see that when sweeping from left to right, the system converges to $D\bar{D}$ solutions until they vanish at the $D\bar{D}$ curve; we note that a $6:5$ and a $6:6$ solution undergo a BCSN bifurcation at the $D\bar{D}$ curve. If the T bifurcation lies to the left of the $D\bar{D}$ curve, then the $1:1$ solution remains stable while the $D\bar{D}$ solutions exist, resulting in regions of multistability. We observe that this behaviour, together with the change in criticality of the BCT bifurcation, is reminiscent of a Chenciner bifurcation, a co-dimension-2 bifurcation that was observed in the smooth system by Keane and Krauskopf³⁶ where it produced rich dynamics.

If the T bifurcation lies to the right of the $D\bar{D}$ curve, this produces regions where vertical stripes can occur between the BCT bifurcation of the $1:1$ solution and the $D\bar{D}$ curve. Note that the vertical stripes do not stretch all the way between the $D\bar{D}$ curve and the BCT bifurcation. There is a second condition that a region must satisfy for the existence of vertical stripes, which is shown by the dashed black curve in Fig. 3. Vertical stripes only occur where the order of D , \bar{D} , H , \bar{H} symbols in the stable solution is consistent with the $1:1$ solution. The difference between stable $P:P$ solutions and the unstable $1:1$ solution they coexist with lies only in the order of Z , \bar{Z} and \bar{H} symbols. This arises because these solutions are generated when Z , H , \bar{Z} and \bar{H} symbols swapped order in the sequence representation of the $1:1$ solution at $\tau = \frac{n}{2}$, $n \in \mathbb{N}$.

V. CONCLUSION

We thoroughly analysed an elementary two-parameter system which combines the effects of time-delayed feedback and periodic forcing. In spite of its simplicity, it demonstrates a complex structure of Arnold tongues with zero-width shrinking points and a high degree of multi-stability. Due to the system being piecewise-linear, we are able to solve the system analytically using an iterative map. We investigate the existence and stability of solutions through the development of a symbolic representation of solutions and the analysis of the subsequently developed Poincaré and border-collision maps. This analysis reveals that the Arnold tongues are bounded by curves of border-collision saddle-node bifurcations of periodic orbits. Additionally, we find curves of torus bifurcations connected to curves of border-collision torus bifurcations, and investigate changes in the criticality of these bifurcations.

Our analysis sheds new light onto previously obtained results in related smooth systems, particularly the El Niño Southern Oscillation climate model studied by Keane, Krauskopf, and Postlethwaite¹⁷. Comparing the numerically calculated bifurcation structure found in that paper with the analytically calculated bifurcation structure found here reveals that the prominent features of the smooth system (1,2) are preserved in the non-smooth limit of $\kappa \rightarrow \infty$. Indeed, the solutions in the smooth system generally appear as “smoothed out” counterparts to the piecewise-linear solutions of the non-smooth system. There are some significant differences. The tongues in the smooth system are not connected by shrinking points, which is to be expected in the presence of nonlinearity, according to Simpson and Meiss³⁷. Additionally, the smooth system contains period doubling bifurcations, which we do not observe in our system, likely due to the loss of nonlinearity in the limit of $\kappa \rightarrow \infty$. However, the analysis presented here does provide new insights into dynamics previously observed numerically^{16,17}.

Both delayed feedback and periodic forcing are very common mathematical model ingredients and can be found in a variety of models used to study, for example, laser dynamics³⁸ and chimera states³⁹. The current work reveals the phenomena which are a genuine consequence of this combination. Therefore, we expect this work to be of interest to a wide readership.

VI. ACKNOWLEDGEMENTS

This research was funded by the Irish Research Council and McAfee LLC through the Irish Research Council Employment-Based Postgraduate Programme. We also thank Dr. Sorcha Healy and the Applied Data Science team at McAfee for their technical support.

VII. APPENDIX

A. Determining legality of a sequence

Each event in a sequence has a time and a position associated with it. The times can be used to generate a system of simultaneous equations:

- Each D occurs at a time $t_D = n$, $n \in \mathbb{Z}$
- Each \bar{D} occurs at a time $t_{\bar{D}} = n + \frac{1}{2}$, $n \in \mathbb{Z}$
- Each H occurs at a time $t_H = t_{\bar{Z}} + \tau$, where $t_{\bar{Z}}$ is a time at which a \bar{Z} occurs
- Each \bar{H} occurs at a time $t_{\bar{H}} = t_Z + \tau$, where t_Z is a time at which a Z occurs
- Each Z is connected to the previous \bar{Z} by the equation showing that the displacement of the trajectory between the two events is 0.
- Each \bar{Z} is connected to the previous Z by the equation showing that the displacement of the trajectory between the two events is 0.

As there is one equation for each symbol, we can solve the system of equation to calculate the times. We then solve for the positions, using the events to calculate the slope between the calculated times. Finally, we generate a set of inequalities for each event:

- The time at which each event occurs must be consistent with the order of sequence.
- Each event occurring between consecutive Z and \bar{Z} events occurs at $x > 0$.
- Each event occurring between consecutive \bar{Z} and Z events occurs at $x < 0$.

If the solved system of equations satisfies the set of inequalities then the sequence is legal, for a given (b, τ) . These techniques allow us to use symbolic sequences to study solutions systematically. Solving for the times and positions associated with events in a sequence, we can plot the solution represented by the sequence. Additionally, by changing the inequalities to equalities, we obtain the bifurcation curves shown in Fig. 3.

B. Calculation of the bifurcation curve of \mathbb{P}

For $\tau > \frac{1}{2}$, \mathbb{P} can be written as

$$\mathbb{P}(S_z) = AS_z + B, \quad (26)$$

where

$$B = \begin{pmatrix} -\frac{1}{2} \\ -\frac{1}{2} \\ -\frac{1}{2} \\ -\frac{1}{2} \\ \dots \\ -\frac{1}{2} \\ \frac{b+2\tau(-1)^{n-1}}{b+(-1)^{n-1}} - \frac{1}{2} \end{pmatrix}. \quad (27)$$

Due to the sparsity of A , the characteristic equation can be readily calculated as

$$(-1 - \lambda)(-\lambda)^{n-1} + (-1)^{n-1} \frac{2(-1)^{n-1}}{b + (-1)^{n-1}} = 0. \quad (28)$$

This simplifies to

$$\lambda^n + \lambda^{n-1} - \frac{2(-1)^{n-1}}{b + (-1)^{n-1}} = 0. \quad (29)$$

By substituting $\lambda = e^{i\rho}$, we can solve for b to determine $b = b_{\text{bif}}$ for which the fixed point of \mathbb{P} is bifurcating as

$$e^{i\rho n} + e^{i\rho(n-1)} - \frac{2(-1)^{n-1}}{b_{\text{bif}} + (-1)^{n-1}} = 0. \quad (30)$$

Note that as $\frac{2(-1)^{n-1}}{b_{\text{bif}} + (-1)^{n-1}} \in \mathbb{R}$,

$$e^{i\rho n} = \overline{e^{i\rho(n-1)}}. \quad (31)$$

So, $e^{i\rho(2n-1)} = 1 = e^{i2\pi k}$, $k \in \mathbb{Z}$, and so $\rho = \frac{2\pi k}{2n-1}$. In order to satisfy Eq. (31), $k = n - 1$. Substituting ρ back into Eq. (30),

$$\cos\left(\frac{2\pi n(n-1)}{2n-1}\right) + \cos\left(\frac{2\pi(n-1)^2}{2n-1}\right) - \frac{2(-1)^{n-1}}{b_{\text{bif}} + (-1)^{n-1}} = 0, \quad (32)$$

which simplifies under a sum-to-product cosine identity to

$$\cos\left(\frac{\pi(n-1)}{2n-1}\right) - \frac{1}{b_{\text{bif}} + (-1)^{n-1}} = 0. \quad (33)$$

Therefore,

$$b_{\text{bif}}(n) = \frac{1}{\cos\left(\frac{\pi(n-1)}{2n-1}\right)} - (-1)^{n-1}, \quad (34)$$

where $n = \lceil 2\tau \rceil$.

REFERENCES

- ¹S. Wicczorek, B. Krauskopf, T. B. Simpson, and D. Lenstra, "The dynamical complexity of optically injected semiconductor lasers," *Phys. Rep.* **416**, 1 (2005).
- ²S. P. Beeby, R. Torah, M. Tudor, P. Glynne-Jones, T. O'donnell, C. Saha, and S. Roy, "A micro electromagnetic generator for vibration energy harvesting," *J. Micromech. Microeng.* **17**, 1257 (2007).
- ³S. Daneshgar, O. De Feo, and M. P. Kennedy, "Observations concerning the locking range in a complementary differential lc injection-locked frequency divider—part I: Qualitative analysis," *IEEE Trans. Circuits Syst. I* **57**, 179 (2010).
- ⁴E. Tziperman, L. Stone, M. A. Cane, and H. Jarosh, "El Niño chaos: Overlapping of resonances between the seasonal cycle and the Pacific ocean-atmosphere oscillator," *Science* **264**, 72 (1994).
- ⁵U. Parlitz and W. Lauterborn, "Superstructure in the bifurcation set of the Duffing equation," *Phys. Lett. A* **107**, 351 (1985).
- ⁶S. Boccaletti, A. N. Pisarchik, C. I. Del Genio, and A. Amann, *Synchronization: from coupled systems to complex networks* (Cambridge University Press, 2018).
- ⁷A. Marchionne, P. Ditlevsen, and S. Wicczorek, "Synchronization vs. resonance: Isolated resonances in damped nonlinear oscillators," *Physica D* **380**, 8 (2018).
- ⁸T. Heil, I. Fischer, W. Elsässer, J. Mulet, and C. R. Mirasso, "Chaos synchronization and spontaneous symmetry-breaking in symmetrically delay-coupled semiconductor lasers," *Phys. Rev. Lett.* **86**, 795 (2001).
- ⁹L. Larger, B. Penkovsky, and Y. Maistrenko, "Virtual chimera states for delayed-feedback systems," *Phys. Rev. Lett.* **111**, 054103 (2013).
- ¹⁰E. Schöll, G. Hiller, P. Hövel, and M. A. Dahlem, "Time-delayed feedback in neurosystems," *Phil. Trans. Royal Soc. A* **367**, 1079 (2009).
- ¹¹J. Runge, V. Petoukhov, and J. Kurths, "Quantifying the strength and delay of climatic interactions: The ambiguities of cross correlation and a novel measure based on graphical models," *J. Climate* **27**, 720 (2014).
- ¹²K. Pyragas, "Control of chaos via extended delay feedback," *Phys. Lett. A* **206**, 323 (1995).
- ¹³J. K. Hale and S. M. V. Lunel, *Introduction to functional differential equations* (Springer Science & Business Media, 1993).
- ¹⁴H. Hu, E. H. Dowell, and L. N. Virgin, "Resonances of a harmonically forced Duffing oscillator with time delay state feedback," *Nonlin. Dynamics* **15**, 311 (1998).
- ¹⁵A. Maccari, "Vibration control for the primary resonance of the van der Pol oscillator by a time delay state feedback," *Int. J. Non-Linear Mechanics* **38**, 123 (2003).
- ¹⁶M. Ghil, I. Zaliapin, and S. Thompson, "A delay differential model of ENSO variability: parametric instability and the distribution of extremes," *Nonlin. Processes Geophys.* **15** (2008).
- ¹⁷A. Keane, B. Krauskopf, and C. Postlethwaite, "Delayed Feedback Versus Seasonal Forcing: Resonance Phenomena in an El Niño Southern Oscillation Model," *SIAM J. Appl. Dyn. Syst.* **14**, 1229 (2015).
- ¹⁸A. Keane, B. Krauskopf, and C. Postlethwaite, "Investigating irregular behavior in a model for the El Niño Southern Oscillation with positive and negative delayed feedback," *SIAM J. Appl. Dyn. Syst.* **15**, 1656 (2016).
- ¹⁹R. D. Nussbaum, "Uniqueness and nonuniqueness for periodic solutions of $\dot{x}(t) = -g(x(t-1))$," *J. Diff. Equ.* **34**, 25 (1979).
- ²⁰S.-N. Chow and H.-O. Walther, "Characteristic multipliers and stability of symmetric periodic solutions of $\dot{x}(t) = -g(x(t-1))$," *Trans. American Math. Soc.* **307**, 127 (1988).
- ²¹Y. Wei-Ming and H. Bai-Lin, "How the Arnold tongues become sausages in a piecewise linear circle map," *Comm. Theo. Phys.* **8**, 1 (1987).
- ²²D. J. W. Simpson and J. D. Meiss, "Shrinking point bifurcations of resonance tongues for piecewise-smooth, continuous maps," *Nonlinearity* **22**, 1123 (2009).
- ²³D. J. W. Simpson, "The structure of mode-locking regions of piecewise-linear continuous maps: I. nearby mode-locking regions and shrinking points," *Nonlinearity* **30**, 382 (2016).
- ²⁴D. J. W. Simpson, "The structure of mode-locking regions of piecewise-linear continuous maps: II. skew sawtooth maps," *Nonlinearity* **31**, 1905 (2018).
- ²⁵N. Metropolis, M. Stein, and P. Stein, "On finite limit sets for transformations on the unit interval," *J. Combinat. Theory, Series A* **15**, 25 (1973).

- ²⁶A. N. W. Hone, M. V. Irle, and G. W. Thurura, “On the Neimark-Sacker bifurcation in a discrete predator-prey system,” *J. Biol. Dyn.* **4**, 594 (2010).
- ²⁷M. di Bernardo, F. Garofalo, L. Iannelli, and F. Vasca, “Bifurcations in piecewise-smooth feedback systems,” *Int. J. of Control* **75**, 1243 (2002).
- ²⁸S. Banerjee and C. Grebogi, “Border collision bifurcations in two-dimensional piecewise smooth maps,” *Phys. Rev. E* **59**, 4052 (1999).
- ²⁹A. Colombo, M. di Bernardo, S. J. Hogan, and M. R. Jeffrey, “Bifurcations of piecewise smooth flows: Perspectives, methodologies and open problems,” *Physica D* **241**, 1845 (2012).
- ³⁰M. di Bernardo, C. Budd, A. Champneys, P. Kowalczyk, A. Nordmark, G. Tost, and P. Piiroinen, “Bifurcations in Nonsmooth Dynamical Systems,” *SIAM Rev.* **50**, 629 (2008).
- ³¹A. Granados, M. Krupa, and F. Clément, “Border Collision Bifurcations of Stroboscopic Maps in Periodically Driven Spiking Models,” *SIAM J. Appl. Dyn. Syst.* **13**, 1387 (2014).
- ³²D. Meiss, “Neimark-Sacker Bifurcations in Planar, Piecewise-Smooth, Continuous Maps,” *SIAM J. Appl. Dyn. Syst.* **7**, 795 (2008).
- ³³H. E. Nusse, E. Ott, and J. A. Yorke, “Border-collision bifurcations: An explanation for observed bifurcation phenomena,” *Phys. Rev. E* **49**, 1073 (1994).
- ³⁴U. Holmberg, *Relay feedback of simple systems.*, Ph.D. thesis, Lund Institute of Technology (1991).
- ³⁵A. Colombo, M. di Bernardo, S. J. Hogan, and P. Kowalczyk, “Complex dynamics in a hysteretic relay feedback system with delay,” *Journal of Nonlinear Science* **17**, 85–108 (2007).
- ³⁶A. Keane and B. Krauskopf, “Chenciner bubbles and torus break-up in a periodically forced delay differential equation,” *Nonlinearity* **31**, R165 (2018).
- ³⁷D. J. W. Simpson and J. D. Meiss, “Resonance near border-collision bifurcations in piecewise-smooth, continuous maps,” *Nonlinearity* **23**, 3091 (2010).
- ³⁸T. Sorrentino, C. Quintero-Quiroz, A. Aragonese, M. C. Torrent, and C. Masoller, “Effects of periodic forcing on the temporally correlated spikes of a semiconductor laser with feedback,” *Opt. Expr.* **23**, 5571 (2015).
- ³⁹V. Semenov, A. Zakharova, Y. Maistrenko, and E. Schöll, “Delayed-feedback chimera states: Forced multiclusters and stochastic resonance,” *EPL* **115**, 10005 (2016).